

**Initialization of a Lattice Boltzmann  
Model with Constrained Runs  
(Extended Version)**

*Pieter Van Leemput*

*Wim Vanroose*

*Dirk Roose*

*Report TW 444, December 2005 (Revised: April 2006)*



**Katholieke Universiteit Leuven**  
Department of Computer Science  
Celestijnenlaan 200A – B-3001 Heverlee (Belgium)

# Initialization of a Lattice Boltzmann Model with Constrained Runs (Extended Version)

*Pieter Van Leemput*

*Wim Vanroose*

*Dirk Roose*

*Report TW 444, December 2005 (Revised: April 2006)*

Department of Computer Science, K.U.Leuven

## Abstract

In this article, we perform a numerical stability and convergence analysis of the constrained runs initialization scheme for a lattice Boltzmann model. Gear and Kevrekidis developed this scheme in the context of coarse-grained equation-free computing. Given the macroscopic initial fields, we study the mapping of these variables to the higher-dimensional space of lattice Boltzmann variables. The lattice Boltzmann model considered is the BGK collision model for one-dimensional reaction-diffusion systems. For such systems, we prove that the constrained runs scheme is unconditionally stable and that it converges to an approximation of the slaved state, i.e. the microscopic state consistent with the macroscopic initial condition. This approximation is correct up to first order in the Chapman-Enskog expansion of the lattice Boltzmann model. The asymptotic convergence factor is  $|1 - \omega|$  with  $\omega$  the BGK relaxation parameter. The results are illustrated for the one-dimensional FitzHugh-Nagumo reaction-diffusion system. Using the constrained runs initialization in the context of equation-free computing, we also perform a coarse-grained bifurcation analysis of this model.

**Keywords** : initialization, lifting, reconstruction, constrained runs, lattice Boltzmann model, coarse-grained equation-free computing.

**AMS(MOS) Classification** : 35K45, 35K57.

# Initialization of a Lattice Boltzmann Model with Constrained Runs (Extended Version)

P. Van Leemput, W. Vanroose and D. Roose

Department of Computer Science, K.U.Leuven, B-3001 Heverlee, Belgium

April 2006

## Abstract

In this article, we perform a numerical stability and convergence analysis of the constrained runs initialization scheme for a lattice Boltzmann model. Gear and Kevrekidis developed this scheme in the context of coarse-grained equation-free computing. Given the macroscopic initial fields, we study the mapping of these variables to the higher-dimensional space of lattice Boltzmann variables. The lattice Boltzmann model considered is the BGK collision model for one-dimensional reaction-diffusion systems. For such systems, we prove that the constrained runs scheme is unconditionally stable and that it converges to an approximation of the slaved state, i.e. the microscopic state consistent with the macroscopic initial condition. This approximation is correct up to first order in the Chapman-Enskog expansion of the lattice Boltzmann model. The asymptotic convergence factor is  $|1-\omega|$  with  $\omega$  the BGK relaxation parameter. The results are illustrated for the one-dimensional FitzHugh-Nagumo reaction-diffusion system. Using the constrained runs initialization in the context of equation-free computing, we also perform a coarse-grained bifurcation analysis of this model.

**Keywords:** initialization, lifting, reconstruction, constrained runs, lattice Boltzmann model, coarse-grained equation-free computing.

**PACS subject classifications:** 02.60.-x, 02.70.-c.

**AMS subject classifications:** 35K45, 35K57.

## 1 Introduction

### 1.1 Initialization of microscopic and mesoscopic models

Complex dynamical systems are often simpler to model on a finer level than the continuum or macroscopic level. Examples are numerous. Molecular dynamics simulations follow the laws of Newton and can be used to model complex fluids such as the flow of polymers. To model e.g. fluid flow at the mesoscopic level, lattice Boltzmann models (LBM) are an alternative to the Navier-Stokes equations. A LBM uses simple collision and propagation rules that update distribution functions of idealized particles on a lattice with limited velocities. We call these fine-level models collectively microscopic models.

However, many of these systems exhibit a separation of time scales between the fast detailed microscopic processes and the slowly varying macroscopic variables. The latter are typically the first few lower order moments of the microscopic variables like density and

velocity fields. Irrespective of the microscopic starting state, time trajectories of such systems are quickly attracted towards a *slow* lower-dimensional *manifold* [10] described by the macroscopic variables. Once on the manifold, the higher order moments of the microscopic variables have become functionals of (become *slaved* by) the lower order ones and the full state is adequately described by the macroscopic variables only. If this description can be written down in closed form, like a set of partial differential equations (PDEs), it is called the *reduced equation* on the manifold. The time needed for the slaving process is called the *healing time* in [16] and is typically small compared to the relevant macroscopic time scales.

In general, starting a microscopic simulator from given macroscopic initial conditions includes some arbitrariness because there are, typically, a large set of microscopic variables and only a few macroscopic variables given (one-to-many problem). In molecular dynamics, for example, the initial positions and velocities of all the particles have to be computed from the given temperature and density profile. Typically, the particles are positioned on a square lattice while the velocities are drawn from a Maxwellian distribution. In a similar way, LBM simulations are traditionally bootstrapped from the initial macroscopic fields by setting the distribution functions in each point to a local equilibrium.

Gear and Kevrekidis proposed the *constrained runs* algorithm in the context of singularly perturbed ODEs [8, 6] to consistently map macroscopic initial data to microscopic variables. In the same context, Zagaris and Kaper compared the scheme, which they call the *zero-derivative principle*, to the computational singular perturbation method [27]. The constrained runs scheme performs a series of short microscopic simulations and resets the lowest moments of the microscopic variables to the macroscopic initial condition after each run while leaving the higher order moments unchanged. After a few iterations, the scheme converges towards an approximation of the slaved state corresponding to the initial macroscopic data. As a result, the microscopic variables are initialized both consistent with the initial macroscopic state and close to the slow manifold described by the macroscopic variables. With such initialization, the subsequent microscopic simulation will approximate the “true” time trajectory (on the manifold) described by the reduced equation.

In this paper, we perform an extensive analysis of the stability and convergence of the constrained runs initialization scheme for the LBM with BGK collisions for one-dimensional diffusive problems. In this context, the initial density  $\rho^{(0)}$  (the lowest moment) is given and we seek the values of the corresponding higher order moments, momentum and energy, (or equivalently, the values of the distribution functions consistent with  $\rho^{(0)}$ ) to initialize the LBM with. We show that the initialization scheme is unconditionally stable and convergent and that the resulting higher order moments are first order accurate. The asymptotic convergence rate equals  $|1 - \omega|$  with  $\omega$  the BGK relaxation parameter.

Only recently, we learned of the related work of Mei *et al.* [17] and Caiazzo [2]. In [17], the authors present a scheme for the initialization of the LBM with multiple relaxation time (MRT) collision model for the incompressible Navier-Stokes problem. For a given initial velocity field  $u^{(0)}$ , both the unknown initial pressure field (or equivalently the density field) and the higher order moments are computed using a modified LBM simulation where the velocity field in the equilibrium distribution is kept fixed to the value  $u^{(0)}$ . This effectively reduces the model to a convection-diffusion LBM with one conserved variable, the density. Caiazzo [2, p. 43] analyzes this scheme for the LBM with BGK collisions for the same Navier-Stokes problem and shows that the resulting pressure (and density) is second order accurate. In this paper, we implement the scheme of [17, 2] for one-dimensional reaction-diffusion systems. We show that it behaves similarly to the constrained runs scheme and that the results of our

numerical analysis also apply to this initialization procedure.

Note that a good initialization is important both in terms of efficiency and accuracy. The simulation of equilibrium systems can be done more efficiently using constrained runs since it eliminates the long run times associated with waiting until an equilibrium sets in. For out-of-equilibrium simulations, such initialization makes it possible to initialize accurately and track the correct transients.

## 1.2 Coarse-grained equation-free computing

The separation of time scales mentioned earlier has inspired Kevrekidis *et al.* to develop so-called *coarse-grained “equation-free”* methods [12] that perform a macroscopic time integration of systems for which only a microscopic model is available. It is assumed that the reduced equation in terms of the macroscopic variables only is (at least conceptually) derivable, but unavailable. The corresponding coarse-grained time stepper performs a macroscopic time step  $\Delta T$  in three phases. In the first phase, called *lifting* or *reconstruction*, the microscopic system is initialized from the macroscopic data. Here, the constrained runs procedure can be used. Secondly, we simulate over  $\Delta T$  using the microscopic model. In the third phase (*restriction*), the macroscopic variables are computed from the resulting microscopic state. Instead of doing a full microscopic simulation, the efficiency of the resulting time stepper can be increased in time by projective integration schemes [7, 26] and in space by gap-tooth techniques [12, 20].

Van Leemput *et al.* showed in [24] that the lifting phase can have a significant impact on the accuracy of the coarse-grained time stepper. For the computation of steady states of a LBM, they showed that a bad initialization of the microscopic simulator can excite slow modes in the system. The macroscopic time step  $\Delta T$  must then be unnecessarily large to damp the resulting initialization error.

For the computation of periodic solutions, such initialization error will induce a permanent phase shift in the solution. Furthermore, when the microscopic simulator is stochastic or chaotic, Makeev *et al.* [15] show that a large  $\Delta T$  leads to irreparable diffusion over a large part of the attractor, thereby losing phase information. It was further shown in the context of numerical bifurcation analysis [24] that the computation of unstable solutions becomes nearly impossible when  $\Delta T$  is very large.

In the context of time integration acceleration schemes as described in [7] and [26], where bursts of microscopic simulations are used to estimate the macroscopic time derivatives, an accurate initialization will limit the size of  $\Delta T$  and efficient schemes can be developed. Finally, the issue of “lifting” also occurs in hybrid domain decomposition techniques where different models are spatially coupled. One example is the coupling of e.g. a PDE to a LBM [1, 25]. At the boundary, the PDE will provide the macroscopic variables from which the LBM distribution functions have to be calculated. This can be seen as a localized initialization that needs to be implemented carefully to ensure smooth behavior of the solution at the interface between the models.

## 1.3 Overview of the paper

In this paper, we apply the constrained runs initialization scheme [8, 6] (see Sect. 3) to the lattice Boltzmann BGK model for one-dimensional reaction-diffusion problems (Sect. 2). In Sect. 4, we will show that the scheme is unconditionally stable and convergent. These

theoretical results are verified numerically in Sect. 5 for the FitzHugh-Nagumo system with no-flux boundary conditions. We also construct the coarse-grained time stepper for this system and use the constrained runs scheme in the lifting phase. We used this time stepper to perform a time stepper based numerical bifurcation analysis of the system [14, 24], although we showed in [23] that coarse-graining the LBM is not a requirement to enable bifurcation analysis (because of the deterministic nature of the mesoscopic LBM). In Sect. 6, we summarize the main conclusions of the paper. In Appendix A, we verify the matrix theorems used to proof stability. Finally, we derive the discrete evolution equations for the moments in an alternative way in Appendix B.

## 2 Lattice Boltzmann Model for One-Dimensional Reaction-Diffusion Systems

Lattice Boltzmann models (LBM) [3, 18] describe the evolution of particle distribution functions  $f_i(x, t)$  discretized in space  $x$ , time  $t$  and velocity  $v_i$ . The distributions are defined on a space-time lattice with grid spacing  $\Delta x$  in space and  $\Delta t$  in time. On a one-dimensional domain, only three values are considered for the velocity (D1Q3 model):

$$v_i = c_i \frac{\Delta x}{\Delta t}, \quad c_i = i \in \{-1, 0, 1\},$$

with  $c_i$  the dimensionless lattice velocity.

The lattice Boltzmann evolution law for the distribution functions is

$$f_i(x + c_i \Delta x, t + \Delta t) = (1 - \omega) f_i(x, t) + \omega f_i^{eq}(x, t) + R_i(x, t), \quad i \in \{-1, 0, 1\}. \quad (1)$$

The right hand side of (1) updates the values  $f_i(x, t)$  to *post-collision* values  $f_i^*(x, t^*)$  (with  $t < t^* < t + \Delta t$ ). Afterwards, these values propagate to a neighboring lattice site according to their velocity direction (left hand side of (1)). When the solution of the LBM varies slowly on a macroscopic length and time scale, the PDE (the reduced equation) describing the same reaction-diffusion process can be derived through a multiscale Chapman-Enskog expansion [25, 3] of (1) and is defined as

$$\frac{\partial \rho(x, t)}{\partial t} = D \frac{\partial^2 \rho(x, t)}{\partial x^2} + F(\rho(x, t)), \quad (2)$$

where  $\rho(x, t)$  is the particle density (concentration),  $D$  the diffusion coefficient and  $F(\rho(x, t))$  a macroscopic reaction force term which depends on  $\rho(x, t)$  only.

Diffusive collisions are modeled by the Bhatnagar-Gross-Krook (BGK) collision term  $-\omega(f_i(x, t) - f_i^{eq}(x, t))$  in (1) as a relaxation to a *local diffusive* equilibrium [19]

$$f_i^{eq}(x, t) = \frac{1}{3} \rho(x, t). \quad (3)$$

The BGK relaxation coefficient  $\omega$  is then defined as [19, 25]

$$\omega = \frac{2}{1 + 3D \frac{\Delta t}{\Delta x^2}}. \quad (4)$$

For stability reasons, it follows from (1) that  $0 < \omega < 2$  [18] (compare (4)).

Reactions are modelled by the term  $R_i(x, t)$  in (1) as [19, 5]

$$R_i(x, t) = \frac{\Delta t}{3} F(\rho(x, t)). \quad (5)$$

Here, it is assumed that reactions occur at the local diffusive equilibrium [4].

The particle density  $\rho(x, t)$  is the macroscopic variable (cf. (2)) and is defined as the zeroth order velocity moment of the distribution functions

$$\rho(x, t) = \sum_{i=-1}^1 f_i(x, t) = \sum_{i=-1}^1 f_i^{eq}(x, t), \quad (6)$$

where the second equality expresses that the BGK diffusive collisions locally conserve density (compare (3)). The dimensionless first and second order velocity moments (up to the factor 1/2 for the second order moment) are

$$\phi(x, t) = \sum_{i=-1}^1 c_i f_i(x, t) \quad ; \quad \xi(x, t) = \frac{1}{2} \sum_{i=-1}^1 c_i^2 f_i(x, t). \quad (7)$$

We will refer to these moments as the ‘‘momentum’’  $\phi$  and (kinetic) ‘‘energy’’  $\xi$  (although these are non-conserved quantities in a diffusive system). The state of the LBM at time  $t$  and position  $x$  is then fully determined by either the distribution functions  $\mathbf{f} = [f_{-1} \ f_0 \ f_1]'$  or the moments  $\boldsymbol{\varrho} = [\rho \ \phi \ \xi]'$ . By definition

$$\begin{bmatrix} \rho \\ \phi \\ \xi \end{bmatrix} = \begin{bmatrix} 1 & 1 & 1 \\ -1 & 0 & 1 \\ \frac{1}{2} & 0 & \frac{1}{2} \end{bmatrix} \begin{bmatrix} f_{-1} \\ f_0 \\ f_1 \end{bmatrix} \quad \Leftrightarrow \quad \boldsymbol{\varrho} = M \mathbf{f} \quad (8)$$

and vice versa  $\mathbf{f} = M^{-1} \boldsymbol{\varrho}$  (one-to-one relationship).

### 3 Initialization with Constrained Runs

#### 3.1 The Slaved State

For the LBM of Sect. 2, the higher order moments  $\phi$  and  $\xi$  are quickly attracted to the slow manifold described by the density  $\rho$  (cf. the discussion in the introduction), i.e. they become quickly slaved to functionals of the macroscopic variable. These functionals (the *slaving relations*) can be derived analytically from the Chapman-Enskog expansion of (1) [25] and are, up to third order, defined as

$$\begin{aligned} \phi(x, t) &= -\frac{2\Delta x}{3\omega} \frac{\partial \rho(x, t)}{\partial x} + \frac{\Delta x \Delta t}{\omega^2} \left( \frac{\omega}{\omega - 2} + \frac{1}{3} \right) \left( \frac{\partial F(\rho(x, t))}{\partial x} - \frac{\partial^2 \rho(x, t)}{\partial x \partial t} \right), \\ \xi(x, t) &= \frac{1}{3} \rho(x, t) - \frac{\Delta t}{6\omega} \left( F(\rho(x, t)) - \frac{\partial \rho(x, t)}{\partial t} \right). \end{aligned} \quad (9)$$

Here, we consider  $\partial/\partial x$  to be a first order operator, while  $\partial/\partial t$  and  $F(\rho)$  are second order contributions (compare (2)). In this way, the above expression for  $\phi$  has a first and third order contribution, while  $\xi$  is written as a combination of zeroth and second order terms. Alternatively, relations (9) can be written in terms of spatial derivatives of  $\rho$  only using (2).

Given only the value of the macroscopic initial condition  $\rho(x, 0)$ , relations (9) can be used to initialize the LBM. First,  $\phi(x, 0)$  and  $\xi(x, 0)$  are computed from  $\rho(x, 0)$  using (9). The derivatives are approximated by finite differences. The corresponding distributions are then obtained as  $\mathbf{f}(x, 0) = M^{-1}\boldsymbol{\varrho}(x, 0)$  (8). Assuming that slaving relations like (9) are unavailable or difficult to obtain analytically, the constrained runs initialization algorithm approximates the values for the missing, slaved higher order moments corresponding to the given macroscopic density.

### 3.2 Constrained Runs Scheme

---

**Algorithm 1** Constrained runs scheme for a one-dimensional diffusive LBM

---

**Required:**  $\rho^{(0)} = \rho(x, 0)$

$$f_i^{(0)} = w_i \rho^{(0)} ; \sum_{i=-1}^1 w_i = 1, \text{ e.g. } w_i = 1/3$$

Choose  $f_i^{(0)}$  s.t. (6) holds

$$\phi^{(0)} = (w_1 - w_{-1})\rho^{(0)} ; \xi^{(0)} = \frac{1}{2}(w_1 + w_{-1})\rho^{(0)}$$

Equiv. higher order moments

**repeat**

$$\mathbf{f}^{(k+1)} = \text{LBM}(\mathbf{f}^{(k)})$$

LBM simulation (1) over time  $\delta t$

$$\boldsymbol{\varrho}^{(k+1)} = M\mathbf{f}^{(k+1)}$$

Corresponding  $\phi^{(k+1)}$  and  $\xi^{(k+1)}$  (8)

$$\rho^{(k+1)} = \rho^{(0)}$$

Reset macroscopic variables

$$\mathbf{f}^{(k+1)} = M^{-1}\boldsymbol{\varrho}^{(k+1)}$$

Map back (8)

**until** convergence heuristic  $< \theta$  , with  $\theta \ll 1$

---

The constrained runs scheme [8, 6] is a fixed point iteration scheme that computes the full state of a microscopic time simulator corresponding to the given macroscopic variables. Using the constrained runs procedure on the LBM from Sect. 2, we iterate upon the higher order moments  $\phi$  and  $\xi$ , given  $\rho$ . We define the constrained runs scheme as a map

$$\boldsymbol{\varrho}^{(k+1)} = \mathcal{C}_{\delta t}(\boldsymbol{\varrho}^{(k)}) ; \quad k = 0, 1, 2, \dots \quad (10)$$

with  $k$  the iteration number and  $\delta t$  the simulation time needed by the inner microscopic simulator. The details for a one-dimensional diffusive LBM are given in Algorithm 1. Although the value  $\rho^{(k)} = \rho^{(0)} = \rho(x, 0)$  is kept constant (reset), we included  $\rho$  in the state vector  $\boldsymbol{\varrho}^{(k)} = [\rho^{(k)} \phi^{(k)} \xi^{(k)}]'$  (8).

A straightforward choice for the convergence heuristic is

$$\|\phi^{(k+1)}(x) - \phi^{(k)}(x)\|_2 < \theta \quad \text{and} \quad \|\xi^{(k+1)}(x) - \xi^{(k)}(x)\|_2 < \theta , \quad (11)$$

with  $\theta$  a user-defined tolerance ( $\theta \ll 1$ ). Note that the computation of the distributions  $\mathbf{f}^{(k+1)} = M^{-1}\boldsymbol{\varrho}^{(k+1)}$  in Algorithm 1 reduces to

$$f_0^{(k+1)} = \rho^{(0)} - f_{-1}^{(k+1)} - f_1^{(k+1)} \quad (12)$$

since solely resetting the density changes the value of  $f_0^{(k+1)}$  only.

Figure 1 sketches the procedure's evolution. We denote the fixed point of the constrained runs scheme by  $\{\tilde{\phi}, \tilde{\xi}\}$  and the corresponding density from the microscopic simulation by  $\tilde{\rho}$ . Due to the microscopic simulation,  $\tilde{\rho}$  will be different from the  $\rho^{(0)}$  to reset to (that is, unless the initial condition is a steady state of the microscopic model itself and  $\tilde{\rho} = \rho^{(0)}$ ). The corresponding higher order moments  $\{\tilde{\phi}, \tilde{\xi}\}$  are only approximations to the missing higher

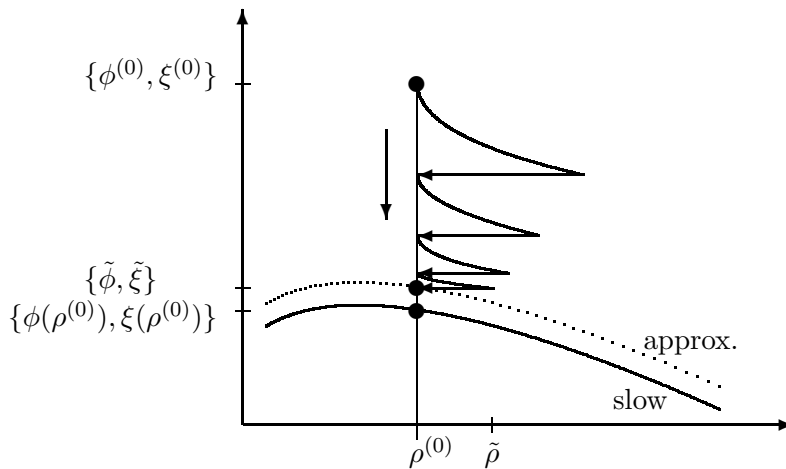


Figure 1: Sketch of the evolution of the constrained runs initialization procedure. The higher order moments  $\phi$  and  $\xi$  are plotted with respect to the macroscopic variable  $\rho$ . The density  $\rho$  is reset to the given  $\rho^{(0)}$  after each LBM simulation. The fixed point  $\{\tilde{\phi}, \tilde{\xi}\}$  of the constrained runs scheme is an approximation to the slaved state  $\{\phi(\rho^{(0)}), \xi(\rho^{(0)})\}$ . The former lies on an “approximate” manifold while the latter lies on the slow manifold described by  $\rho$ . The value  $\tilde{\rho}$  is the density corresponding to  $\{\tilde{\phi}, \tilde{\xi}\}$  (before the final reset to  $\rho^{(0)}$ ) and will be useful as an estimate for the error.

order moments  $\{\phi(\rho^{(0)}), \xi(\rho^{(0)})\}$  of the slaved state. The values  $\{\rho^{(0)}, \tilde{\phi}, \tilde{\xi}\}$  denote a point on an “approximate” manifold instead of the true slow manifold described by the density  $\rho$  (cf. Fig. 1). Since the approximation error is proportional to the microscopic simulation time  $\delta t$ , the latter should be chosen as small as possible. For a LBM, we thus choose  $\delta t = \Delta t$  (one LBM time step).

## 4 Analysis of the Constrained Runs Scheme

In Sect. 4.1, we derive the equations that couple the evolution of the moments  $\rho$ ,  $\phi$  and  $\xi$  at the current position  $x$ . In Sect. 4.2, we prove that the constrained runs scheme for the LBM for one-dimensional reaction-diffusion systems is unconditionally stable. As a corollary of the proof, we also derive the asymptotic convergence factor. Finally, we show in Sect. 4.3 that the constrained runs scheme converges to an approximation of the slaved state.

### 4.1 Evolution Equations in the Space of Moments

In order to obtain a time stepper for the distribution functions  $f_i(x, t)$  evaluated at the *current* position  $x$ , the standard LBM BGK equation (1) can be written alternatively as

$$f_i(x, t + \Delta t) = (1 - \omega) f_i(x - c_i \Delta x, t) + \omega f_i^{eq}(x - c_i \Delta x, t) + R_i(x - c_i \Delta x, t). \quad (13)$$

Expanding the terms in the right hand side of (13) up to second order around respectively  $f_i(x, t)$ ,  $f_i^{eq}(x, t)$  and  $R_i(x, t)$ , we obtain

$$\begin{aligned} f_i(x, t + \Delta t) = & (1 - \omega) \left( f_i(x, t) - c_i \Delta x \frac{\partial f_i(x, t)}{\partial x} + \frac{c_i^2 \Delta x^2}{2} \frac{\partial^2 f_i(x, t)}{\partial x^2} \right) \\ & + \omega \left( f_i^{eq}(x, t) - c_i \Delta x \frac{\partial f_i^{eq}(x, t)}{\partial x} + \frac{c_i^2 \Delta x^2}{2} \frac{\partial^2 f_i^{eq}(x, t)}{\partial x^2} \right) \\ & + R_i(x, t) - c_i \Delta x \frac{\partial R_i(x, t)}{\partial x} + \frac{c_i^2 \Delta x^2}{2} \frac{\partial^2 R_i(x, t)}{\partial x^2}. \end{aligned} \quad (14)$$

We now transform (14) to the space of moments. First, we sum over all distributions. Using definitions (8), we then get the equation for the macroscopic variables  $\rho$

$$\begin{aligned} \rho(x, t + \Delta t) = & \rho(x, t) + (1 - \omega) \left( -\Delta x \frac{\partial \phi(x, t)}{\partial x} + \Delta x^2 \frac{\partial^2 \xi(x, t)}{\partial x^2} \right) \\ & + \frac{\omega \Delta x^2}{3} \frac{\partial^2 \rho(x, t)}{\partial x^2} + \Delta t F(\rho(x, t)) + \frac{\Delta t \Delta x^2}{3} \frac{\partial^2 F(\rho(x, t))}{\partial x^2}, \end{aligned} \quad (15)$$

where we used property (6) (local conservation of density), definitions (3) and (5) and  $c_1^2 = c_{-1}^2 = 1$ . The evolution equation for momentum  $\phi$  is derived by multiplying (14) with  $c_i$  and summing over all  $i$

$$\begin{aligned} \phi(x, t + \Delta t) = & (1 - \omega) \left( \phi(x, t) - 2 \Delta x \frac{\partial \xi(x, t)}{\partial x} + \frac{\Delta x^2}{2} \frac{\partial^2 \phi(x, t)}{\partial x^2} \right) \\ & - \frac{2 \omega \Delta x}{3} \frac{\partial \rho(x, t)}{\partial x} - \frac{2 \Delta x \Delta t}{3} \frac{\partial F(\rho(x, t))}{\partial x}. \end{aligned} \quad (16)$$

If we multiply (14) by  $c_i^2/2$  and sum afterwards, we get the following equation for energy  $\xi$

$$\begin{aligned} \xi(x, t + \Delta t) = & (1 - \omega) \left( \xi(x, t) - \frac{\Delta x}{2} \frac{\partial \phi(x, t)}{\partial x} + \frac{\Delta x^2}{2} \frac{\partial^2 \xi(x, t)}{\partial x^2} \right) + \frac{\omega}{3} \rho(x, t) \\ & + \frac{\omega \Delta x^2}{6} \frac{\partial^2 \rho(x, t)}{\partial x^2} + \frac{\Delta t}{3} F(\rho(x, t)) + \frac{\Delta t \Delta x^2}{6} \frac{\partial^2 F(\rho(x, t))}{\partial x^2}. \end{aligned} \quad (17)$$

Obviously, the explicit time stepping in the above equations can be seen as a forward finite difference discretization of the corresponding continuous time derivative. Therefore, substituting  $\boldsymbol{\rho}(x, t + \Delta t) - \boldsymbol{\rho}(x, t) = \Delta t \partial \boldsymbol{\rho}(x, t) / \partial t$  in (15)–(17) leads to the fully continuous versions (in  $x$  and  $t$ ) of these equations.

Note that the reduced PDE (2) is obtained by substituting the slaving relations (9) for  $\phi$  and  $\xi$  up to first order into (15) and retaining only the terms up to second order.

## 4.2 Stability Analysis

The eigenvalues of the linearization (i.e. the Jacobian matrix) of the constrained runs scheme (10) will determine its stability. Section 4.2.1 lists a few theorems about the eigenvalues of a certain class of matrices that will be needed further on. In Sect. 4.2.2 and 4.2.3, we derive the Jacobian matrix for the LBM under discussion with either periodic, no-flux or Dirichlet boundary conditions. Finally, we prove in Sect. 4.2.4 that the scheme is unconditionally stable for the type of systems considered.

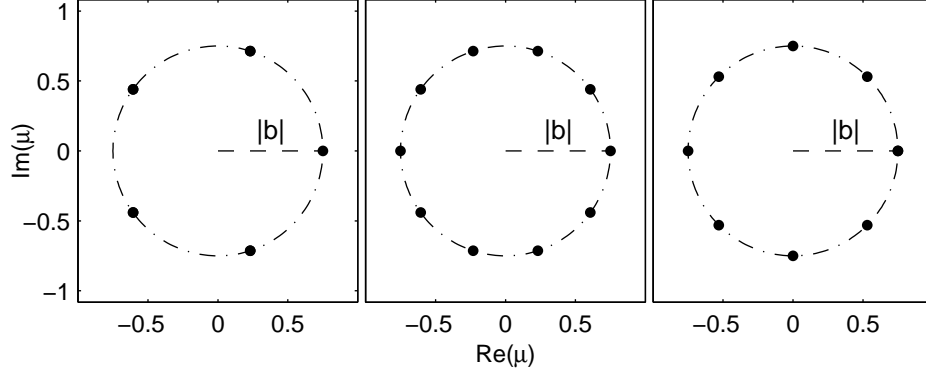


Figure 2: Eigenvalues  $\mu_m$  of the  $10 \times 10$  matrices with structure (18) (left), (20) (middle) or (21) (right) and relations (19) for  $b = 0.75$ .

#### 4.2.1 Useful Matrix Lemmas

Here, we state a few general lemmas about the eigenvalue spectra of a class of matrices that will be needed in Sect. 4.2.4. The proofs are given in Appendix A. Figure 2 shows the numerically computed eigenvalues  $\mu$  of matrices (18), (20) and (21). The matrix elements are related as in (19) with  $b = 0.75$ .

**Lemma 1.** *Define a square  $2N \times 2N$  matrix  $J$  structured as follows (here given a small dimensional example with  $2N = 10$ ):*

$$\begin{bmatrix}
 & & a & -b & & & & & a & b \\
 & & -c & a & & & & & c & a \\
 a & b & & & a & -b & & & & \\
 c & a & & & -c & a & & & & \\
 & & a & b & & a & -b & & & \\
 & & c & a & & -c & a & & & \\
 & & & & a & b & & & a & -b \\
 & & & & c & a & & & -c & a \\
 a & -b & & & & & a & b & & \\
 -c & a & & & & & c & a & & 
 \end{bmatrix} \quad (18)$$

(for clarity, we omitted zeros from our notation). When the elements of such a matrix are related as

$$a = \frac{b}{2} \quad ; \quad c = \frac{b}{4} \quad ; \quad b \in \mathbb{R}, \quad (19)$$

the matrix has  $N$  distinct eigenvalues  $\mu_m = b \exp(im 2\pi/N)$ ;  $m = 0, 1, \dots, N - 1$  (each with multiplicity 2), which lie on a circle with radius  $|b|$ .





**No-flux boundary conditions** No-flux boundary conditions are best implemented using the halfway bounce-back scheme [9, 11]. This puts the LBM variables at the midpoints of  $N$  lattice intervals. Consider the left boundary, which is a distance  $\Delta x/2$  away from the nearest internal site  $x_1$ . The halfway bounce-back implementation states that the unknown incoming (out-of-wall) distribution  $f_1$  is given by

$$f_1(x_1, t + \Delta t) = f_{-1}^*(x_1, t), \quad (28)$$

a condition which is imposed during propagation.

The discrete evolution equation for momentum at the left boundary site  $x_1$  can be written as

$$\phi(x_1, t + \Delta t) = f_1(x_1, t + \Delta t) - f_{-1}(x_1, t + \Delta t) \quad (29)$$

$$= f_{-1}^*(x_1, t) - f_{-1}^*(x_2, t) \quad (30)$$

$$= (1 - \omega)f_{-1}(x_1, t) - (1 - \omega)f_{-1}(x_2, t) + G(\rho(x_1, t); \rho(x_2, t)) \quad (31)$$

$$= -\frac{(1 - \omega)}{2}\phi(x_1, t) + (1 - \omega)\xi(x_1, t) + \frac{(1 - \omega)}{2}\phi(x_2, t) \\ - (1 - \omega)\xi(x_2, t) + G(\rho(x_1, t); \rho(x_2, t)) \quad (32)$$

$$= -a\phi(x_1, t) + b\xi(x_1, t) + a\phi(x_2, t) - b\xi(x_2, t) + G(\rho(x_1, t); \rho(x_2, t)). \quad (33)$$

Equation (29) defines the momentum (7) after propagation. Imposing propagation and the boundary condition (28), we obtain (30). Enforcing BGK collisions and reactions, (31) is obtained in terms of the pre-collision distributions. Substituting the corresponding pre-collision higher order moments using  $\mathbf{f} = M^{-1}\boldsymbol{\rho}$  (8), (32) and (33) are obtained, the latter using (26). The term  $G$  gathers the terms depending on  $\rho$ . This term winds up in the vector of constants (23) and does not contribute to the Jacobian matrix. The coefficients in (33) are precisely the elements in the first row of matrix (20). The second row follows from a similar derivation for the energy.

The same type of derivation can be done for the rightmost site  $x_N$  (where  $f_{-1}(x_N, t + \Delta t) = f_1^*(x_N, t)$ ) to obtain the coefficients in the last two rows of (20).

**Dirichlet boundary conditions** To enforce Dirichlet boundary conditions, we put the  $N$  lattice points at the edges of  $N - 1$  intervals, such that the boundaries coincide with the outer lattice sites  $x_1$  and  $x_N$ . Note that  $\Delta x$  is now  $L/(N - 1)$  with  $L$  the domain length. The unknown distributions at the boundaries are computed during propagation as

$$f_1(x_1, t + \Delta t) = \rho(x_1, t) - f_0^*(x_1, t) - f_{-1}^*(x_2, t), \\ f_{-1}(x_N, t + \Delta t) = \rho(x_N, t) - f_0^*(x_N, t) - f_1^*(x_{N-1}, t), \quad (34)$$

where  $\rho(x_1, t)$  and  $\rho(x_N, t)$  are the density values imposed by the Dirichlet condition at the boundary.

The discrete evolution equation for momentum at the left boundary site  $x_1$  can be written

as

$$\phi(x_1, t + \Delta t) = f_1(x_1, t + \Delta t) - f_{-1}(x_1, t + \Delta t) \quad (35)$$

$$= \rho(x_1, t) - f_0^*(x_1, t) - 2f_{-1}^*(x_2, t) \quad (36)$$

$$= -(1 - \omega)f_0(x_1, t) - 2(1 - \omega)f_{-1}(x_2, t) + G(\rho(x_1, t); \rho(x_2, t)) \quad (37)$$

$$= -(1 - \omega)\rho(x_1, t) + 2(1 - \omega)\xi(x_1, t) + (1 - \omega)\phi(x_2, t) - 2(1 - \omega)\xi(x_2, t) + G(\rho(x_1, t); \rho(x_2, t)) \quad (38)$$

$$= 2(1 - \omega)\xi(x_1, t) + (1 - \omega)\phi(x_2, t) - 2(1 - \omega)\xi(x_2, t) + G'(\rho(x_1, t); \rho(x_2, t)) \quad (39)$$

$$= 2b\xi(x_1, t) + b\phi(x_2, t) - 2b\xi(x_2, t) + G'(\rho(x_1, t); \rho(x_2, t)) . \quad (40)$$

The reasoning is equivalent to the one for equations (29)–(33). Again, the terms  $G$  and  $G'$  gather the terms depending on  $\rho$ . The coefficients in (40) are the elements in the first row of matrix (21). The second row follows from a similar derivation for the energy. The last two rows are derived from the same type of derivation for the rightmost site  $x_N$ .

#### 4.2.4 Stability Theorem

**Theorem 1 (Stability theorem).** *The constrained runs scheme for the lattice Boltzmann BGK model that describes a one-dimensional reaction-diffusion system with either periodic, no-flux or Dirichlet boundary conditions (and with the reaction term depending on  $\rho$  only (5)), is unconditionally stable.*

*Proof.* The eigenvalues  $\mu_m$  of the linearization (the Jacobian matrix) of one iteration of the fixed point map  $\mathcal{C}_{\Delta t}$  (10) determine the stability of the algorithm. If all eigenvalues in the spectrum  $\sigma(\mathcal{C}_{\Delta t})$  lie within the unit circle, i.e.  $\forall \mu_m \in \sigma(\mathcal{C}_{\Delta t}) : |\mu_m| < 1$ , the iteration is stable.

Since (26) satisfies (19), the Jacobian matrix in (25) represents the bulk of the matrix  $J$  (except for the boundaries) from either Lemmas 1, 2 or 3. Depending on the type of boundary conditions (see Sect. 4.2.3), the full structure of  $J$  given in (18), (20) or (21) is obtained. These theorems state that all eigenvalues  $\mu_m$  lie on a circle centered at the origin with radius  $|b| = |1 - \omega|$ . The constrained runs iteration is unconditionally stable because, as already mentioned in Sect. 2,  $0 < \omega < 2$  and thus always  $|\mu_m| = |b| < 1$ .  $\square$   $\square$

**Theorem 2 (Asymptotic convergence factor).** *The asymptotic convergence factor  $\eta$  of the constrained runs scheme for the LBM described in Theorem 1 equals  $|1 - \omega|$ .*

*Proof.* The proof of Theorem 1 states that all eigenvalues  $\mu_m$  lie on a circle with radius  $|b| = |1 - \omega|$ . Hence the spectral radius (or equivalently, the asymptotic convergence factor) is given by

$$\eta := \max_{\mu_m \in \sigma(\mathcal{C}_{\Delta t})} |\mu_m| = |b| = |1 - \omega| .$$

$\square$

$\square$

### 4.3 Convergence

**Theorem 3 (Convergence theorem).** *The constrained runs scheme for the LBM described in Theorem 1 converges to a first order correct approximation  $\{\tilde{\phi}, \tilde{\xi}\}$  of the slaved state (9). The approximation error depends on  $\tilde{\rho} - \rho^{(0)}$ , where  $\rho^{(0)}$  is the initial density and  $\tilde{\rho}$  is the internal simulated-upon density corresponding to  $\{\tilde{\phi}, \tilde{\xi}\}$  (before the final reset to  $\rho^{(0)}$ ).*

*Proof.* The unconditional stability of the constrained runs algorithm (Theorem 1) implies that the scheme converges to a fixed point  $\{\tilde{\phi}, \tilde{\xi}\}$ . We will now prove that this is an approximation to the slaved state (9).

Since the macroscopic variable  $\rho$  is reset in each step of the algorithm, i.e. since  $\rho^{(k+1)} = \mathcal{C}_{\Delta t}([\rho^{(0)} \phi^{(k)} \xi^{(k)}]')$ , equation (15) becomes

$$\begin{aligned} \rho^{(k+1)} = & \rho^{(0)} + (1 - \omega) \left( -\Delta x \frac{\partial \phi^{(k)}}{\partial x} + \Delta x^2 \frac{\partial^2 \xi^{(k)}}{\partial x^2} \right) + \frac{\omega \Delta x^2}{3} \frac{\partial^2 \rho^{(0)}}{\partial x^2} \\ & + \Delta t F(\rho^{(0)}) + \frac{\Delta t \Delta x^2}{3} \frac{\partial^2 F(\rho^{(0)})}{\partial x^2} \end{aligned} \quad (41)$$

after simulation in the  $(k+1)^{th}$  step. Reordering terms in (41), we obtain an expression for the term between brackets. Substituting this expression in (17) results in the following equation for  $\xi^{(k+1)}$ :

$$\xi^{(k+1)} = \xi^{(k)} - \omega \xi^{(k)} + \frac{\omega}{3} \rho^{(0)} - \frac{\Delta t}{6} F(\rho^{(0)}) + \frac{1}{2} (\rho^{(k+1)} - \rho^{(0)}). \quad (42)$$

The fixed point  $\{(\rho^{(0)}), \tilde{\phi}, \tilde{\xi}\}$  of (10) is defined by  $\tilde{\phi}^{(k+1)} = \tilde{\phi}^{(k)}$  and  $\tilde{\xi}^{(k+1)} = \tilde{\xi}^{(k)}$ . Denote the corresponding density from simulation by  $\tilde{\rho}$  (cf. Fig. 1). In the fixed point, (42) equals

$$\tilde{\xi} = \frac{1}{3} \rho^{(0)} - \frac{\Delta t}{6 \omega} F(\rho^{(0)}) + \frac{1}{2 \omega} (\tilde{\rho} - \rho^{(0)}). \quad (43)$$

When we substitute (43) in (16), the following equation for the fixed point value  $\tilde{\phi}$  can be derived

$$\begin{aligned} \tilde{\phi} = & -\frac{2 \Delta x}{3 \omega} \frac{\partial \rho^{(0)}}{\partial x} + \left( \frac{1}{3} - \omega \right) \frac{\Delta t \Delta x}{\omega^2} \frac{\partial F(\rho^{(0)})}{\partial x} - (1 - \omega) \frac{\Delta x}{\omega^2} \frac{\partial (\tilde{\rho} - \rho^{(0)})}{\partial x} \\ & + (1 - \omega) \frac{\Delta x^2}{2 \omega} \frac{\partial^2 \tilde{\phi}}{\partial x^2}. \end{aligned} \quad (44)$$

An expression for  $\partial^2 \tilde{\phi} / \partial x^2$  is obtained by derivation of (44) and keeping only the lowest (third) order terms. Using (2), this can be written as

$$\frac{\partial^2 \tilde{\phi}}{\partial x^2} = -\frac{2 \Delta x}{3 \omega} \frac{\partial^3 \rho^{(0)}}{\partial x^3} = \frac{2}{(\omega - 2) \Delta x} \left( \frac{\partial (\tilde{\rho} - \rho^{(0)})}{\partial x} - \Delta t \frac{\partial F(\rho^{(0)})}{\partial x} \right). \quad (45)$$

Substituting (45) in (44), we finally obtain

$$\tilde{\phi} = -\frac{2 \Delta x}{3 \omega} \frac{\partial \rho^{(0)}}{\partial x} + \frac{\Delta x \Delta t}{\omega^2} \left( \frac{\omega}{\omega - 2} + \frac{1}{3} \right) \frac{\partial F(\rho^{(0)})}{\partial x} - \frac{\Delta x}{\omega^2} \left( \frac{\omega}{\omega - 2} + 1 \right) \frac{\partial (\tilde{\rho} - \rho^{(0)})}{\partial x}. \quad (46)$$

When we compare (43) and (46) to the analytic slaving relations for momentum and energy given in (9), we see that the first two terms match, but not the third one. Using the notion of order from Sect. 3.1, it follows that the fixed point  $\{(\rho^{(0)}), \tilde{\phi}, \tilde{\xi}\}$  matches the slaved state (9) completely up to first order. Using (8), this is equivalent to stating that the corresponding fixed point distribution functions  $\tilde{f}_i$  are a first order correct approximation of the  $f_i$  in the Chapman-Enskog expansion of (1) or (13) (see [25]). The approximation error

is proportional to the error made upon resetting the density, i.e. the value  $\tilde{\rho} - \rho^{(0)}$  and the spatial derivative thereof. This value is thus a measure for the “difference” between the slow manifold and the actual approximate manifold converged upon (see Fig. 1).

Note that in a full system steady state, i.e. a steady state of the LBM itself, the approximation error in (43) and (46) vanishes since all time derivatives (and thus also  $\tilde{\rho} - \rho^{(0)}$ ) evaluate to zero. As already mentioned in [8], this means that full system steady states lie both on the approximate and the slow manifold.

As discussed in Sect. 3, choosing the smallest possible simulation time  $\delta t$  ensures that the error in (43) and (46) is as small as possible. Also, the error is small when the density profile is smooth.  $\square$   $\square$

## 5 Numerical Results

In Sect. 5.2, we illustrate the theoretical results from Sect. 4 for the FitzHugh-Nagumo (FHN) reaction-diffusion system with no-flux boundary conditions. The details of this system are given in Sect. 5.1. A related initialization scheme developed by Mei *et al.* [17, 2] is discussed in Sect. 5.3 for our model problem. In Sect. 5.4, we use the constrained runs scheme as the lifting procedure in the coarse-grained time stepper for the FHN LBM and perform a time stepper based numerical bifurcation analysis of the resulting system.

### 5.1 Example: FitzHugh-Nagumo Reaction-Diffusion System

There are two species in the FHN system: the activator and inhibitor, denoted by the superscripts *ac* and *in* respectively. For each species, the LBM is described in Sect. 2. We discretize the one-dimensional spatial domain  $[0, 20]$  with  $N = 200$  lattice points. At the boundaries, we impose no-flux boundary conditions which are implemented using the halfway bounce-back scheme [9, 11]. This puts the lattice points at the midpoints of  $N$  lattice intervals ( $\Delta x = 0.1$ ). We use a LBM time step  $\Delta t = 0.001$  [24]. The evolution of the species is coupled through the reaction terms  $R_i(x, t)$  only, which are defined as (5)

$$\begin{aligned} R_i^{ac}(x, t) &= \frac{\Delta t}{3} (\rho^{ac}(x, t) - (\rho^{ac})^3(x, t) - \rho^{in}(x, t)) , \\ R_i^{in}(x, t) &= \frac{\Delta t}{3} \varepsilon (\rho^{ac}(x, t) - a_1 \rho^{in}(x, t) - a_0) . \end{aligned} \tag{47}$$

The parameters values are  $a_0 = -0.03$  and  $a_1 = 2$ , while the diffusion coefficients in (4) are  $D^{ac} = 1$  and  $D^{in} = 4$ . We chose  $\varepsilon = 0.05$  in all our numerical experiments, except for Sect. 5.4, where we performed pseudo-arclength continuation with free parameter  $\varepsilon \in [0, 1]$ . The equivalent reduced PDE equations (2) can be found in e.g. [22, 24].

### 5.2 Stability and Convergence

First, we computed the Jacobian matrix  $J$  of the constrained runs procedure numerically using a finite difference technique. Column  $l$  of  $J$  is obtained as the directional derivative of  $\mathcal{C}_{\Delta t}(\boldsymbol{\varrho}^{(k)})$  (10) in the direction of the  $l^{\text{th}}$  unit vector  $e_l$  using

$$J[l] = J e_l = \frac{\mathcal{C}_{\Delta t}(\boldsymbol{\varrho}^{(k)} + \varepsilon e_l) - \mathcal{C}_{\Delta t}(\boldsymbol{\varrho}^{(k)})}{\varepsilon} ,$$

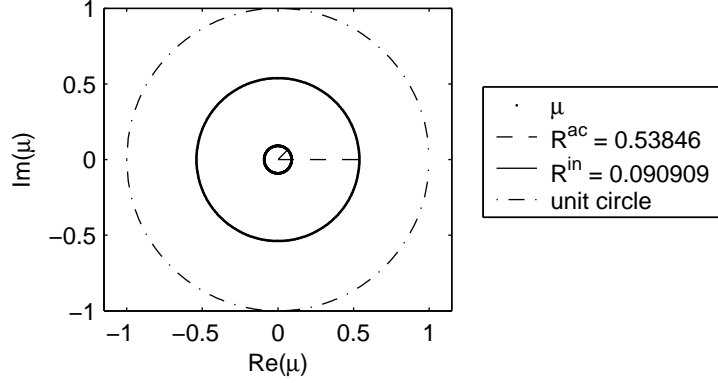


Figure 3: Eigenvalues  $\mu$  of the Jacobian matrix of the constrained runs scheme for the FHN LBM problem. The smallest circle of  $2N = 400$  eigenvalues corresponds to the inhibitor species, while the larger circle of 400 eigenvalues is related to the activator species. The unit circle represents the stability boundary. The computed values for the circle radii  $R^{ac}$  and  $R^{in}$  are given also.

where  $\epsilon$  is a small parameter.

For the FHN model with two species, we use the following ordering of the state vector  $\boldsymbol{\rho}^{(k)} = [\rho^{ac} \rho^{in} \phi^{ac} \xi^{ac} \phi^{in} \xi^{in}]'$  (where we omitted the iteration index  $k$ ). The resulting Jacobian matrix  $J$  has the following structure

$$\begin{bmatrix} I & 0 & 0 \\ B^{ac} & A^{ac} & \mathbf{0} \\ B^{in} & \mathbf{0} & A^{in} \end{bmatrix} \quad (48)$$

where each sparse submatrix is  $2N \times 2N$  dimensional. The identity matrix  $I$  is related to both species' densities, while the submatrices  $A^{ac}$ ,  $B^{ac}$  and  $A^{in}$ ,  $B^{in}$  are associated with both  $\phi$  and  $\xi$  for either the activator or inhibitor species. If the discretized state variables  $\phi$  and  $\xi$  are written in an interwoven manner (24) or if permutations are done on the Jacobian, these matrices are banded ( $2 \times 2$  block tridiagonal) with bandwidth 6. The submatrices  $B^{ac}$  and  $B^{in}$  contain the derivatives of the  $\phi$ - and  $\xi$ -equations with respect to  $\rho$  and can be worked out analytically from  $B_{cont}$  (23) or equivalently from  $B_{disc}$  (25).

Note that the marked submatrices in (48) which gather the derivatives that couple the higher order moments of the activator with the higher order moments of the inhibitor and vice versa, are zero matrices. This means that there is no extra coupling between the activator and inhibitor higher order moments other than the one induced by momentum and energy quickly becoming slaved with respect to their own species' density, which is in turn the only variable coupled to the other species. This is in agreement with (47) (and the corresponding force term in the reduced PDEs) where the species' densities are coupled through the reaction term only.

The eigenvalues of the block lower triangular matrix (48) are the eigenvalues of each diagonal block. The density-related identity matrix  $I$  accounts for  $2N$  eigenvalues  $\mu = 1$  which do not count for the stability/convergence analysis since  $\rho$  is kept constant by constraining (resetting) its value. Since  $\rho$  is not really a state variable, the corresponding eigenvalues are neglected.

Both submatrices  $A^{ac}$  and  $A^{in}$  are structured as in (20) (with relations (26)). Lemma 2

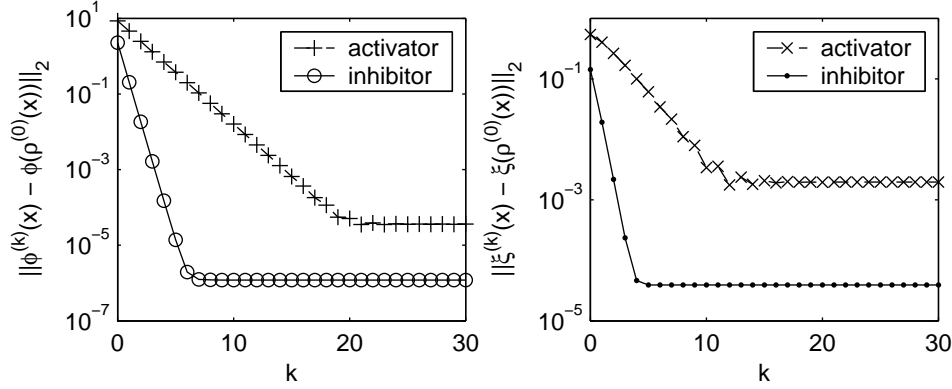


Figure 4: Convergence of the higher order moments  $\phi^{(k)}$  and  $\xi^{(k)}$  in the constrained runs scheme with respect to the “unknown” slaved higher order moments  $\phi(\rho^{(0)})$  and  $\xi(\rho^{(0)})$ . To better show linear convergence, we initialized Algorithm 1 with a bad choice for the higher order moments  $\phi^{(0)} = -0.74\rho^{(0)}$  and  $\xi^{(0)} = 0.38\rho^{(0)}$ .

states that each matrix has  $2N$  eigenvalues lying on a circle. Figure 3 shows the numerically computed eigenvalues of the Jacobian matrix of the constrained runs procedure evaluated at the fixed point  $\{(\rho^{(0)}), \tilde{\phi}, \tilde{\xi}\}$ . The circles of eigenvalues have radius  $R^{ac} = 0.53846 < 1$  and  $R^{in} = 0.090909 < 1$  respectively. It can be checked that all eigenvalues lie at equi-angular distances  $\pi/N$  on the circle, which is conform Lemma 2. The constrained runs iteration is stable because all eigenvalues lie within the unit circle.

Substituting the parameter values of our model problem in (4), we see that

$$\omega^{ac} = 1.53846 \quad \text{and} \quad \omega^{in} = 0.90909 ,$$

such that

$$b^{ac} = 1 - \omega^{ac} = -0.53846 \quad \text{and} \quad b^{in} = 1 - \omega^{in} = 0.090909 . \quad (49)$$

In absolute value, these are exactly the radii  $R^{ac}$  and  $R^{in}$  computed in Fig. 3.

Figure 4 shows the evolution of the higher order moments  $\phi^{(k)}$  and  $\xi^{(k)}$  computed in the constrained runs procedure with respect to the “missing” higher order moments  $\phi(\rho^{(0)})$  and  $\xi(\rho^{(0)})$  of the starting point. The latter were obtained by first simulating with the LBM until slaving is obtained, i.e. over a time interval larger than the healing time, here  $20\Delta t$  [24] (cf. the discussion in the introduction) and then computing the  $\phi$  and  $\xi$  values (7) that correspond to the resulting  $\rho^{(0)}$  (the starting point for this experiment). The asymptotic convergence factor  $\eta$  can be estimated as

$$\eta^\kappa = \frac{\|E^{(k+\kappa)}\|_2}{\|E^{(k)}\|_2} ; \quad \kappa = 1, 2, \dots , \quad (50)$$

with  $E^{(k)}$  the error at step  $k$ , i.e. either  $E^{(k)} = \phi^{(k)} - \phi(\rho^{(0)})$  or  $E^{(k)} = \xi^{(k)} - \xi(\rho^{(0)})$ . Computing (50) for the momentum variables leads to values  $\eta^{ac} \approx 0.53$  and  $\eta^{in} \approx 0.090$  (Fig. 4 left), while for the energy variables  $\eta^{ac} \approx 0.60$  and  $\eta^{in} \approx 0.11$  (Fig. 4 right). These values are approximations to the respective theoretical asymptotic convergence factors (circle radii)  $|b^{ac}|$  and  $|b^{in}|$  (49). Since  $|b^{in}| < |b^{ac}|$ , the inhibitor species converges faster.

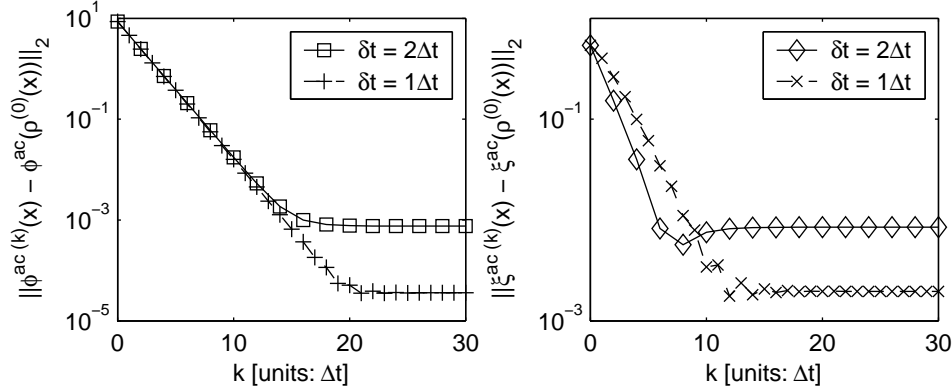


Figure 5: Convergence plots of the constrained runs procedure for the activator species. The LBM simulation is performed for  $\delta t = \Delta t$  or  $\delta t = 2\Delta t$ . The initial condition in Algorithm 1 is  $\phi^{(0)} = -0.74\rho^{(0)}$  and  $\xi^{(0)} = 0.38\rho^{(0)}$ . The left panel shows the evolution of momentum  $\phi^{ac(k)}$ , while the right panel shows the evolution of energy  $\xi^{ac(k)}$  with respect to the corresponding “unknown” slaved moments. Output is shown at the same absolute time, thus we slightly abuse the index  $k$  notation.

To verify expressions (43) and (46) numerically, we computed the norm of the difference between  $\xi$ , respectively  $\tilde{\phi}$ , and the right hand side of (43) and (46) evaluated at the  $\tilde{\rho}$  and  $\rho^{(0)}$  values. We obtained values within machine precision.

The convergence plots in Fig. 4 level off because the fixed point  $\{\tilde{\phi}, \tilde{\xi}\}$  ends up on the approximate manifold instead of the true slow manifold (cf. Sect. 3). The simple convergence heuristic (11) does not take this “levelling off” into account. However, the error terms in (43) and (46) suggest to monitor the differences  $\rho^{(k+1)} - \rho^{(0)}$  and the spatial derivative thereof for  $k = 0, 1, 2, \dots$  and stop iterating when these values converge (since  $\tilde{\rho} - \rho^{(0)}$  is a measure for the difference between the approximate manifold and the slow manifold at  $\rho^{(0)}$ ). Figure 4 shows that about 25 iterations are sufficient if  $\rho^{(k+1)} - \rho^{(0)}$  is monitored. This is conform our experiments. Note that the simulation overhead incurred by the constrained runs initialization comes at the benefit of a very accurate time simulation afterwards (see Sect. 5.4).

The absolute stability of the constrained runs procedure implies that the scheme is always convergent, independent of the initial condition in Algorithm 1. A bad choice of  $f_i^{(0)}$  (or equivalently  $\phi^{(0)}$  and  $\xi^{(0)}$ ) away from the slaving relations (9) leads to a larger initial error  $E^{(0)}$  and thus a few more iterations necessary for convergence. The fixed point converged upon is however the same. To better show linear convergence in Fig. 4, we chose the distributions asymmetrically as  $f_{-1}^{(0)} = 0.75\rho^{(0)}$ ,  $f_0^{(0)} = 0.24\rho^{(0)}$ ,  $f_1^{(0)} = 0.01\rho^{(0)}$  (or  $\phi^{(0)} = -0.74\rho^{(0)}$  and  $\xi^{(0)} = 0.38\rho^{(0)}$ ) instead of the better option of e.g.  $f_i^{(0)} = \rho^{(0)}/3$  (or  $\phi^{(0)} = 0$  and  $\xi^{(0)} = \rho^{(0)}/3$ ), where the latter is closer to the slaved state.

Figure 5 illustrates that it is best to choose the simulation time  $\delta t$  of the microscopic simulator used in the constrained runs scheme (10) as small as possible. In case of a LBM thus equal to one  $\Delta t$ . Results are shown for  $\delta t$  either equal to  $\Delta t$  or  $2\Delta t$ . Although the latter initially converges faster, the fixed point of the former is more accurate.

### 5.3 Comparison to the Initialization Scheme of Mei *et al.*

Mei *et al.* [17] proposed an initialization scheme for the LBM MRT model for the incompressible Navier-Stokes problem. Caiazzo [2] analyzes this scheme for the LBM BGK model for

---

**Algorithm 2** Initialization of Mei *et al.* for one-dimensional diffusive LBM
 

---

**Required:**  $\rho^{(0)} = \rho(x, 0)$ 

$$f_i^{(0)} = \rho^{(0)}/3$$

 Initialize with e.g. the BGK equilibrium  $f_i^{eq}$ 
**repeat**

$$\mathbf{f}^{(k+1)} = \text{LBM}_{\text{mod}}(\mathbf{f}^{(k)}, \rho^{(0)})$$

 Run modified LBM over time  $\Delta t$ 
**until** convergence heuristic  $< \theta$ , with  $\theta \ll 1$ 

$$\tilde{\phi} = M\tilde{\mathbf{f}}$$

 Corresponding  $\tilde{\phi}$  and  $\tilde{\xi}$  (8)

$$\tilde{\rho} = \rho^{(0)}$$

Use initial density

$$\tilde{\mathbf{f}} = M^{-1}\tilde{\phi}$$

 Corresponding distribution functions (8)
 

---

the same Navier-Stokes problem. We implement this initialization scheme for the LBM BGK model for one-dimensional diffusive problems. The LBM from Sect. 2 is then initialized with Algorithm 2. Here, evolution equation  $\text{LBM}_{\text{mod}}(\mathbf{f}^{(k)}, \rho^{(0)})$  represents (1) with a fixed density value  $\rho^{(0)}$  in both the equilibrium distribution and reaction term, i.e. (3) and (5) are replaced with

$$f_i^{eq}(x, t) = \frac{1}{3}\rho^{(0)}(x, t) \quad ; \quad R_i(x, t) = \frac{\Delta t}{3}F(\rho^{(0)}(x, t)) . \quad (51)$$

Note that for diffusion, this is not a LBM anymore, since density is not conserved by the BGK collisions, i.e. the second equality in (6) does not hold. This implies that the converged distributions  $\tilde{f}_i$  do not sum up to the correct initial density  $\rho^{(0)}$ . A small additional transformation is necessary (last lines of Algorithm 2).

We now compare Algorithms 1 and 2. The constrained runs scheme uses the LBM itself and manipulates the distribution functions externally by resetting the macroscopic variables to the given initial fields. On the other hand, the scheme of Mei *et al.* modifies the LBM internally by fixing the macroscopic variables to the initial values in the equilibrium distribution and force terms. The resulting scheme relaxes towards the given macroscopic variables.

However, it can be checked that the evolution of  $\phi$  and  $\xi$  (or equivalently  $f_1$  and  $f_{-1}$ ) is the same in both Algorithms 1 and 2. Indeed, in step  $k$  of Algorithm 1, we reset the density (12). In step  $k + 1$ , the density – which is a conserved variable here – is computed (6) and used in the BGK equilibrium (3) and reaction term (5) in (1). The resulting iteration for  $f_1$  and  $f_{-1}$  is equal to (1) with (51). Note that for  $f_0$ , the schemes behave differently, which is the reason for the reset of density in the last lines of Algorithm 2. We can conclude that the higher order moments have the same convergence behavior (this can be checked numerically also). Thus the results of Theorems 1, 2 and 3 apply. As a consequence, the converged higher order moments  $\tilde{\phi}$  and  $\tilde{\xi}$  for our model problem in Algorithm 2 are first order accurate and their values are given by (43) and (46).

## 5.4 Application: Coarse-Grained Numerical Bifurcation Analysis

Next, we use the constrained runs procedure in the *lifting (reconstruction)* step of the coarse-grained time stepper [12] for our LBM. We compare our results to those obtained with the reconstruction scheme proposed in [22]

$$f_i(x, 0) = w_i \rho(x, 0) \quad \text{with} \quad \sum_{i=-1}^1 w_i = 1 . \quad (52)$$

As discussed in [24], this type of initialization does not attempt to approximate the slaving relations (9) for the higher order moments. This induces a significant macroscopic error, which leads to an unnecessary large value of  $\Delta T$ . The best possible approximation to the slaving relations with (52) is the choice  $w_i = 1/3$ , i.e. initialization with the local diffusive BGK equilibrium (3). The corresponding initial higher order moments are  $\xi = \rho/3$  (good) and  $\phi = 0$  (bad, although the numerical value is small also). After initialization, we simulate over a coarse-grained time step  $\Delta T$  using the LBM. Finally, the *restriction* computes  $\rho(x, t + \Delta T)$  using (6). To focus on the effect of the lifting only, these  $\Delta T$ -integrations are successively repeated within the time integration interval  $[0, T]$ , instead of using this basic time stepper in combination with more advanced time integration acceleration techniques [7, 26].

We have used this coarse-grained LBM time stepper in a time stepper based numerical bifurcation analysis using the Newton-Picard method [14]. For the FHN model with the choice of parameters mentioned in Sect. 5.1, we compute a branch of steady states and a branch of periodic solutions for varying  $\varepsilon \in [0, 1]$ . Figure 6 shows the results for the coarse-grained LBM with either the reconstruction scheme (52) with  $w_i = 1/3$  or the constrained runs procedure (Algorithm 1). We compare to the bifurcation diagram of the full LBM (without coarse-graining) [23]. For steady states, we set  $T = 5$ , while for periodic solutions,  $T$  is the period. We choose  $\Delta T = 20\Delta t = 0.02$  (on the order of the healing time [24]). It is clear from Fig. 6 that, even for such small value of  $\Delta T$ , the results for the constrained runs initialization compare well to those for the full LBM, which is not the case for the reconstruction with (52) and  $w_i = 1/3$ . Note that we failed to compute the complete periodic solution branch in the direction of the fold point for the reconstruction with  $f_i(x, 0) = (1/3)\rho(x, 0)$  (52). The resulting time stepper proved too inaccurate to compute solutions near the unstable ones beyond the fold point.

## 6 Conclusions

In this paper, we analyzed the use of the constrained runs scheme [8, 6] for the initialization of a lattice Boltzmann model (LBM) from given macroscopic initial fields. The LBM considered is the BGK model for one-dimensional reaction-diffusion systems with either periodic, no-flux or Dirichlet boundary conditions. For such systems, we proved that the constrained runs scheme is unconditionally stable and convergent. We showed that the scheme converges to a first order correct approximation of the slaved state, i.e. the state that is consistent with the macroscopic initial condition. Furthermore, we derived that the asymptotic convergence factor equals  $|1 - \omega|$ , with  $\omega$  the BGK relaxation coefficient. We used the FitzHugh-Nagumo reaction-diffusion system with no-flux boundary conditions to illustrate the theoretical results.

We also used the constrained runs scheme as the lifting or reconstruction step in the coarse-grained time stepper [12] for the LBM and performed a time stepper based numerical bifurcation analysis [14, 24] of the result. We showed that the resulting bifurcation diagram is very accurate, even if the coarse-grained time step is small.

As an alternative to constrained runs, the initialization scheme of Mei *et al.* [17, 2] can be used. For the LBM BGK model for one-dimensional reaction-diffusion systems, we showed that this initialization procedure is very similar and that the results of our numerical analysis apply, yielding the same convergence and accuracy results.

Although initialization of the microscopic model with the constrained runs scheme incurs some extra work compared to a direct initialization with e.g. the local BGK equilibrium

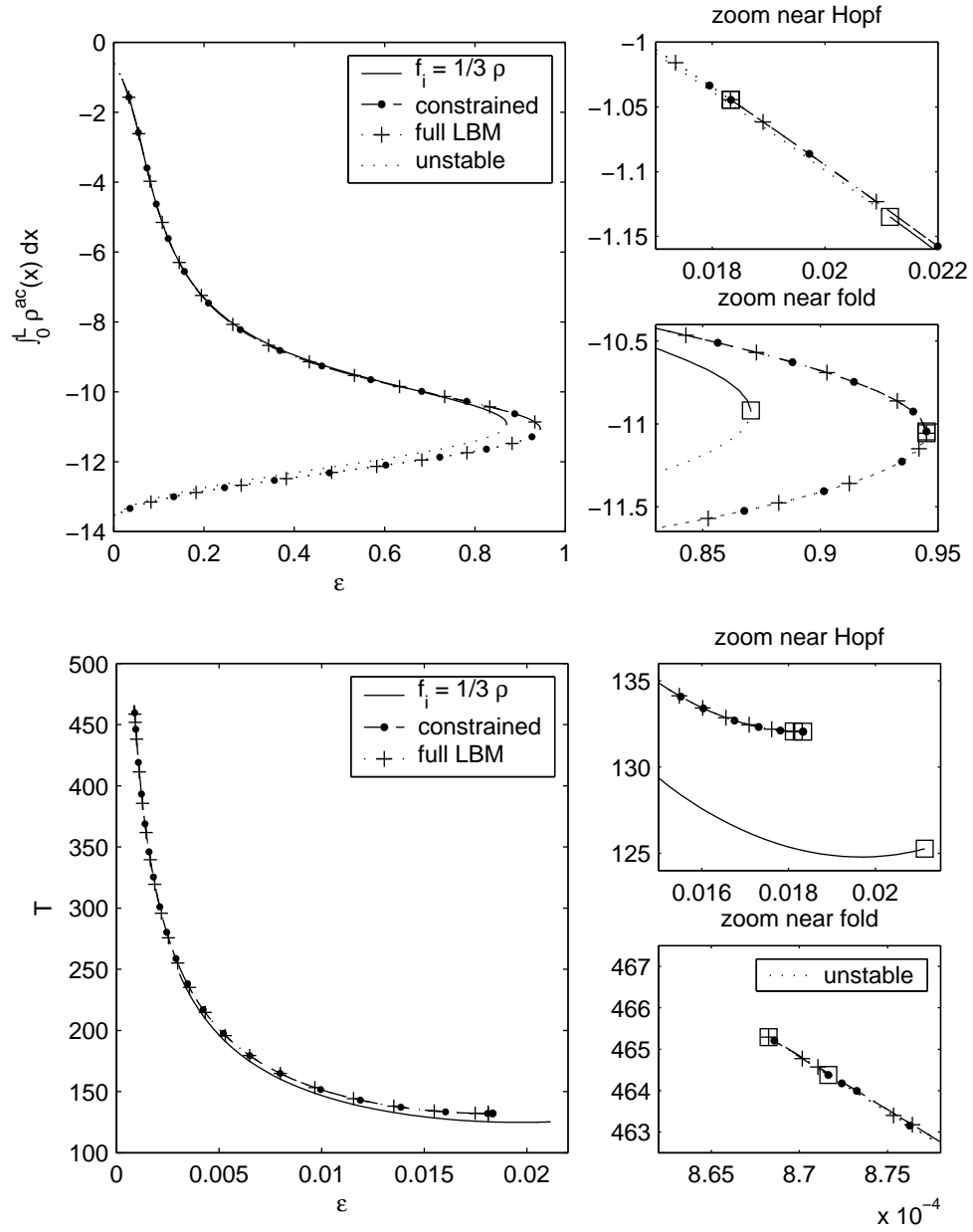


Figure 6: Bifurcation diagram for steady states (top) and periodic solutions (bottom). Time steppers are the coarse-grained LBM with reconstruction scheme either  $f_i(x, 0) = (1/3)\rho(x, 0)$  (52) or the constrained runs scheme (Algorithm 1) and the full LBM for reference. Unstable solutions are indicated by dotted lines and bifurcation points by boxed markers. The markers represent only a subset of the computed points.

distribution, the benefits are clear. After initialization, the microscopic state is both consistent with the initial macroscopic state and close to the slow manifold described by the macroscopic variables. On the contrary, initialization with the BGK equilibrium can lead to significant macroscopic initialization errors, as shown in [24] and [17, 2].

For the microscopic model itself, an accurate initialization will reduce the simulation time and allows for the computation of meaningful transients. In the context of equation-free computing, a proper initialization is an important issue for coarse-grained time integration acceleration [7, 26], bifurcation analysis [24] and hybrid domain decomposition techniques [25].

We believe that the numerical analysis in this article can be extended to lattice Boltzmann BGK models for higher dimensional systems and systems other than reaction-diffusion also. Although it seems unlikely that the eigenvalues of the linearized constrained runs scheme for a more general LBM lie on a circle, the factor  $(1 - \omega)$  can still be expected to play an important role in the stability analysis. Below, we comment on the generalization of this analysis.

To start with, the general BGK term in the LBM equation can still be expanded in a Taylor series. Deriving the continuous evolution equations in the higher order moments is however less straightforward. To this end, a meaningful set of higher order moments must be defined. For e.g. a two dimensional problem, the definitions in [13] can be useful here. Note that the discretization of the spatial derivatives in these equations should be the natural one corresponding to the nearest neighbor nature of the propagation (cf. Appendix B). This will result in a sparsity pattern of the corresponding Jacobian matrix comparable to the one in this paper. Also, since the BGK equilibrium distribution only depends on the macroscopic variables which are kept constant during the constrained iterations, this term will not contribute to the Jacobian matrix, i.e. it will not contribute to the stability analysis.

## Acknowledgements

We thank prof. K. Lust for his feedback on the numerical bifurcation analysis, prof. M. Van Barel for his help with the proofs in Appendix A and prof. I.G. Kevrekidis for providing us with early versions of [8, 6]. The work of P. Van Leemput is supported by project G.0130.03 funded by the Fund for Scientific Research - Flanders. This paper presents research results of the Belgian Programme on Interuniversity Attraction Poles, initiated by the Belgian Federal Science Policy Office, who also provide funding for W. Vanroose with a DWTC return grant.

## A Proofs of the Matrix Lemmas from Sect. 4.2.1

### A.1 Proof of Lemma 1

The  $2N \times 2N$  matrix  $J$  (18) can be written as

$$J = b \hat{J} , \tag{53}$$

such that the corresponding eigenvalues are related as

$$\mu = b \hat{\mu} . \tag{54}$$

We will now prove that the eigenvalues  $\hat{\mu}$  of  $\hat{J}$  lie on the unit circle with angular distance  $2\pi/N$ .

Both matrices  $J$  (18) and  $\hat{J}$  (53) are so-called *compound-circulant* matrices. From [21] it follows that the eigenvalues  $\hat{\mu}$  of  $\hat{J}$  can be found as the union of eigenvalues  $\lambda$  of the  $2 \times 2$  matrices

$$H_m = \begin{bmatrix} 1/2 & -1 \\ -1/4 & 1/2 \end{bmatrix} r_m + \begin{bmatrix} 1/2 & 1 \\ 1/4 & 1/2 \end{bmatrix} r_m^{N-1}, \quad (55)$$

where  $r_m$  is any  $N^{\text{th}}$  root of unity:

$$r_m = \exp(i m \frac{2\pi}{N}) = \cos(m \frac{2\pi}{N}) + i \sin(m \frac{2\pi}{N}); \quad m = 0, 1, 2, \dots, N-1. \quad (56)$$

The eigenvalues  $\lambda$  of  $H_m$  are the roots of the characteristic equation  $\det(H_m - \lambda I) = 0$  (with  $I$  the  $2 \times 2$  unit matrix), i.e.

$$\lambda^2 - (r_m + r_m^{N-1})\lambda + 1 = 0.$$

Using definition (56) and the fact that the complex conjugate  $\overline{r_m} = r_m^{N-1} = r_{N-m}$ , it is readily found that

$$\lambda_{1,m} = r_m \quad \text{and} \quad \lambda_{2,m} = \overline{r_m} = r_{N-m}. \quad (57)$$

Since these eigenvalues are defined for any  $r_m$ , it follows that  $\hat{\mu}_m = r_m$ ;  $m = 0, 1, \dots, N-1$ , each with multiplicity 2. Multiplying these eigenvalues by  $b$  to obtain  $\mu_m$  (54) proves the theorem.

## A.2 Proof of Lemma 2

For the matrix  $J$  in (20), we will prove that the eigenvalues  $\hat{\mu}$  of the corresponding matrix  $\hat{J}$  (53) are the  $2N^{\text{th}}$  roots of unity  $\hat{\mu}_m = \exp(i m \pi/N)$ ;  $m = 0, 1, \dots, 2N-1$ . Since (54) holds, this will prove the theorem. In practice, we have to prove that the characteristic equation of  $\hat{J}$  equals

$$p(\lambda) = \lambda^{2N} - 1 = 0. \quad (58)$$

By definition, the roots of  $p(\lambda) = 0$  are the eigenvalues  $\hat{\mu}$  of  $\hat{J}$ . First, we prove that

$$p(\hat{J}) = \hat{J}^{2N} - I = 0 \quad (59)$$

holds (where  $I$  is now the  $2N \times 2N$  unit matrix).

Define the  $2 \times 2$  submatrices  $\alpha$ ,  $\beta$ ,  $\gamma$  and  $\delta$  as

$$\alpha = \begin{bmatrix} -1/2 & 1 \\ -1/4 & 1/2 \end{bmatrix}; \quad \beta = \begin{bmatrix} 1/2 & -1 \\ -1/4 & 1/2 \end{bmatrix}; \quad \gamma = \begin{bmatrix} 1/2 & 1 \\ 1/4 & 1/2 \end{bmatrix}; \quad \delta = \begin{bmatrix} -1/2 & -1 \\ 1/4 & 1/2 \end{bmatrix}. \quad (60)$$

One can compute the multiplication table 1 for the matrices (60). For the example  $2N = 10$ , the powers of the compound matrix  $\hat{J}$  (see (61) and compare  $(1/b)J$  (20)) are

$$\hat{J} = \begin{bmatrix} \alpha & \beta & & & \\ \gamma & & \beta & & \\ & \gamma & & \beta & \\ & & \gamma & & \beta \\ & & & \gamma & \delta \end{bmatrix}; \quad \hat{J}^9 = \begin{bmatrix} \delta & \gamma & & & \\ \beta & & \gamma & & \\ & \beta & & \gamma & \\ & & \beta & & \gamma \\ & & & \beta & \alpha \end{bmatrix} \quad (61)$$

Table 1: Multiplication table for the  $2 \times 2$  matrices  $\alpha, \beta, \gamma$  and  $\delta$  (60)

$\cdot$	$\alpha$	$\beta$	$\gamma$	$\delta$
$\alpha$	0	$\alpha$	0	$\gamma$
$\beta$	0	$\beta$	0	$\delta$
$\gamma$	$\alpha$	0	$\gamma$	0
$\delta$	$\beta$	0	$\delta$	0

$$\hat{J}^2 = \begin{bmatrix} & \alpha & \beta & & \\ \alpha & & & \beta & \\ \gamma & & & & \beta \\ & \gamma & & \delta & \\ & & \gamma & \delta & \end{bmatrix} ; \quad \hat{J}^8 = \begin{bmatrix} & & \delta & \gamma & & \\ \delta & & & & \gamma & \\ \beta & & & & & \gamma \\ & \beta & & & & \alpha \\ & & \beta & \alpha & & \end{bmatrix} \quad (62)$$

$$\hat{J}^3 = \begin{bmatrix} & & \alpha & \beta & & \\ \alpha & & & \beta & & \\ \gamma & & & \delta & & \\ & \gamma & & \delta & & \\ & & \gamma & \delta & & \end{bmatrix} ; \quad \hat{J}^7 = \begin{bmatrix} & & & \delta & \gamma & \\ \delta & & & & \gamma & \\ \beta & & & & \alpha & \\ & \beta & & & & \alpha \\ & & \beta & \alpha & & \end{bmatrix} \quad (63)$$

$$\hat{J}^4 = \begin{bmatrix} & & & \alpha & \beta & \\ \alpha & & & \delta & & \\ \gamma & & & & \delta & \\ & \alpha & & \delta & & \\ & & \alpha & \delta & & \end{bmatrix} ; \quad \hat{J}^6 = \begin{bmatrix} & & & & \delta & \gamma \\ & & & \delta & & \alpha \\ & & \delta & & & \alpha \\ \delta & & & \alpha & & \\ \beta & \alpha & & & & \end{bmatrix} \quad (64)$$

$$\hat{J}^5 = \begin{bmatrix} & & & & & \alpha + \delta \\ & & & & \alpha + \delta & \\ & & & \alpha + \delta & & \\ & & \alpha + \delta & & & \\ \alpha + \delta & & & & & \end{bmatrix} \quad (65)$$

It can be checked that  $\hat{J}^{2N} = \hat{J}^{10} = I$ , which proves (59).

Secondly, we prove that there is no polynomial  $q(\lambda)$  with degree less than  $2N$  such that  $q(\hat{J}) = 0$ . Define  $q(\lambda)$  as

$$d_{2N-1}\lambda^{2N-1} + d_{2N-2}\lambda^{2N-2} + \dots + d_2\lambda^2 + d_1\lambda + d_0, \quad (66)$$

with arbitrary coefficients  $d_n$ ;  $n = 0, 1, \dots, 2N - 1$ . From the structure of the powers of  $\hat{J}$  (61)–(65), it follows that  $q(\hat{J}) = 0$  holds if and only if

$$\begin{aligned} d_n\alpha + d_{2N-n}\delta &= 0 & ; & & d_n\gamma + d_{2N-n}\beta &= 0 ; \\ d_n\delta + d_{2N-n}\alpha &= 0 & ; & & d_n\beta + d_{2N-n}\gamma &= 0 . \end{aligned} \quad (67)$$

Equations (67) hold only when  $d_n = 0$ ;  $\forall n = 1, \dots, 2N - 1$ . Thus there is no polynomial like (66) which makes  $q(\hat{J}) = 0$ . We conclude that  $p(\lambda)$  (58) is the sole monic polynomial of degree  $2N$  which is annihilated by  $\hat{J}$ . As a consequence of the Cayley-Hamilton theorem, we can then state that (58) is indeed the characteristic equation of  $\hat{J}$ .

### A.3 Numerical Verification of Conjecture 3

We will verify Conjecture 3 numerically, without giving a formal proof for the derivation of the characteristic equation. We have to show that the eigenvalues  $\hat{\mu}$  of  $\hat{J}$  (53) for  $J$  (21) are the  $2N - 2$  roots of unity, complemented with two extra eigenvalues  $\hat{\mu}_0 = 1$ , or equivalently, that these  $\hat{\mu}$  values are the roots of the following equation

$$p(\lambda) = (\lambda - 1)^2(\lambda^{2N-2} - 1) = 0. \quad (68)$$

If (68) is the characteristic equation of  $\hat{J}$ , the Cayley-Hamilton theorem states that  $\hat{J}$  satisfies the same equation, i.e.

$$p(\hat{J}) = (\hat{J} - I)^2(\hat{J}^{2N-2} - I) = 0. \quad (69)$$

Note that eigenvalue  $\hat{\mu}_0 = 1$  can be found directly in both the second and last row of matrix  $\hat{J} = J/b$  (21). When dropping both the second and last rows and columns, the resulting  $(2N - 2) \times (2N - 2)$  matrix should satisfy  $(\lambda^{2N-2} - 1) = 0$ . This (and (69)) can be verified numerically for arbitrary  $N$  using e.g. MATLAB<sup>®</sup>. The numerically computed eigenvalues  $\hat{\mu}$  satisfy (68). Using (54), the eigenvalues  $\mu$  of  $J$  are found.

## B Discrete Evolution Equations for the Moments

In Sect. 4.1, we derived the continuous evolution equations for  $\rho$ ,  $\phi$  and  $\xi$  using a second order Taylor series expansion of (13). In Sect. 4.2, we discretized these equations using standard central differences in order to obtain the elements in the corresponding Jacobian matrix. Here, we describe a discrete alternative derived directly from the LBM. The key element is writing the moments after propagation  $\mathbf{g}(x_j, t + \Delta t)$  as a function of the moments before collisions  $\mathbf{g}(x_{j-i}, t)$ . Away from the boundaries in lattice sites  $x_j$ ,  $j = 2, \dots, N - 1$ , the momentum after one LBM time step  $\Delta t$  can be written as

$$\phi(x_j, t + \Delta t) = f_1(x_j, t + \Delta t) - f_{-1}(x_j, t + \Delta t) \quad (70)$$

$$= f_1^*(x_{j-1}, t) - f_{-1}^*(x_{j+1}, t) \quad (71)$$

$$= (1 - \omega)(f_1(x_{j-1}, t) - f_{-1}(x_{j+1}, t)) + \frac{\omega}{3}(\rho(x_{j-1}, t) - \rho(x_{j+1}, t)) \\ + \frac{\Delta t}{3}(F(\rho(x_{j-1}, t)) - F(\rho(x_{j+1}, t))) \quad (72)$$

$$= \frac{(1 - \omega)}{2}(\phi(x_{j-1}, t) + \phi(x_{j+1}, t)) + (1 - \omega)(\xi(x_{j-1}, t) - \xi(x_{j+1}, t)) \\ + \frac{\omega}{3}(\rho(x_{j-1}, t) - \rho(x_{j+1}, t)) + \frac{\Delta t}{3}(F(\rho(x_{j-1}, t)) - F(\rho(x_{j+1}, t))). \quad (73)$$

Equation (70) is just the definition of momentum after propagation. Propagation of distributions to the neighboring sites according to their velocity direction leads to (71). As in Sect. 2,  $f_i^*$  denotes the value of the post-collision (or pre-propagation) distribution with velocity  $c_i$ . By imposing BGK collisions and reactions as in (1), (72) is obtained. Rewriting (72) as a function of the pre-collision moments using  $\mathbf{f} = M^{-1}\mathbf{g}$  (8), we obtain (73).

The same type of derivation can be done for the energy after one time step, leading to

$$\xi(x_j, t + \Delta t) = \frac{1}{2}(f_1(x_j, t + \Delta t) + f_{-1}(x_j, t + \Delta t)) \quad (74)$$

$$= \frac{1}{2}(f_1^*(x_{j-1}, t) + f_{-1}^*(x_{j+1}, t)) \quad (75)$$

$$= \frac{(1-\omega)}{2}(f_1(x_{j-1}, t) + f_{-1}(x_{j+1}, t)) + \frac{\omega}{6}(\rho(x_{j-1}, t) + \rho(x_{j+1}, t)) \\ + \frac{\Delta t}{6}(F(\rho(x_{j-1}, t)) + F(\rho(x_{j+1}, t))) \quad (76)$$

$$= \frac{(1-\omega)}{4}(\phi(x_{j-1}, t) - \phi(x_{j+1}, t)) + \frac{(1-\omega)}{2}(\xi(x_{j-1}, t) + \xi(x_{j+1}, t)) \\ + \frac{\omega}{6}(\rho(x_{j-1}, t) + \rho(x_{j+1}, t)) + \frac{\Delta t}{6}(F(\rho(x_{j-1}, t)) + F(\rho(x_{j+1}, t))). \quad (77)$$

Using relations (26), it can be seen that (73) and (77) precisely make up the Jacobian matrix (25). Writing (73) and (77) respectively as

$$\phi(x_j, t + \Delta t) = (1-\omega) \left( \phi(x_j, t) + \frac{1}{2}(\phi(x_{j+1}, t) - 2\phi(x_j, t) + \phi(x_{j-1}, t)) \right) \\ - \frac{2(1-\omega)}{2}(\xi(x_{j+1}, t) - \xi(x_{j-1}, t)) - \frac{2\omega}{6}(\rho(x_{j+1}, t) - \rho(x_{j-1}, t)) \\ - \frac{2\Delta t}{6}(F(\rho(x_{j+1}, t)) - F(\rho(x_{j-1}, t))), \quad (78)$$

$$\xi(x_j, t + \Delta t) = -\frac{(1-\omega)}{4}(\phi(x_{j+1}, t) - \phi(x_{j-1}, t)) \\ + (1-\omega) \left( \xi(x_j, t) + \frac{1}{2}(\xi(x_{j+1}, t) - 2\xi(x_j, t) + \xi(x_{j-1}, t)) \right) \\ + \frac{\omega}{3}\rho(x_j, t) + \frac{\omega}{6}(\rho(x_{j+1}, t) - 2\rho(x_j, t) + \rho(x_{j-1}, t)) \\ + \frac{\Delta t}{3}F(\rho(x_j, t)) + \frac{\Delta t}{6}(F(\rho(x_{j+1}, t)) - 2F(\rho(x_j, t)) + F(\rho(x_{j-1}, t))), \quad (79)$$

we obtain the discretization by central differences of (16) and (17). The discrete version of the evolution equation for  $\rho$  (15) can be obtained in the same way.

## References

- [1] P. Albuquerque, D. Alemani, B. Chopard, and P. Leone. Coupling a lattice Boltzmann and a finite difference scheme. In M. Bubak, G. D. van Albada, P. M. Soot, and J. Dongarra, editors, *International Conference on Computational Science – ICCS 2004*, volume 3039 of *Lecture Notes in Computer Science*, pages 540–547. Springer-Verlag, 2004.
- [2] A. Caiazzo. Analysis of lattice Boltzmann initialization routines. *Journal of Statistical Physics*, 121(1-2):37–48, October 2005.
- [3] B. Chopard, A. Dupuis, A. Masselot, and P. Luthi. Cellular automata and lattice Boltzmann techniques: An approach to model and simulate complex systems. *Advances in Complex Systems*, 5(2/3):103–246, 2002.

- [4] D. Dab, J.-P. Boon, and Y.-X. Li. Lattice-gas automata for coupled reaction-diffusion equations. *Physical Review Letters*, 66(19):2535–2538, 1991.
- [5] S. P. Dawson, S. Chen, and G. D. Doolen. Lattice Boltzmann computations for reaction-diffusion equations. *Journal of Chemical Physics*, 98(2):1514–1523, 1993.
- [6] C. W. Gear, T. J. Kaper, I. G. Kevrekidis, and A. Zagaris. Projecting to a slow manifold: Singularly perturbed systems and legacy codes. *SIAM Journal on Applied Dynamical Systems*, 4(3):711–732, 2005.
- [7] C. W. Gear and I. G. Kevrekidis. Projective methods for stiff differential equations: Problems with gaps in their eigenvalue spectrum. *SIAM Journal on Scientific Computing*, 24(4):1091–1106, 2003.
- [8] C. W. Gear and I. G. Kevrekidis. Constraint-defined manifolds: A legacy code approach to low-dimensional computation. *Journal of Scientific Computing*, 25(1):17–28, 2005. can also be obtained from arXiv e-Print archive as physics/0312094.
- [9] I. Ginzbourg and P. M. Adler. Boundary flow condition analysis for the three-dimensional lattice Boltzmann model. *Journal of Physics II France*, 4:191–214, 1994.
- [10] A. N. Gorban and I. V. Karlin. *Invariant Manifolds for Physical and Chemical Kinetics*. Lecture Notes in Physics. Springer, 2005.
- [11] X. He, Q. Zou, L.-S. Luo, and M. Dembo. Analytic solutions of simple flows and analysis of nonslip boundary conditions for the lattice Boltzmann BGK model. *Journal of Statistical Physics*, 87(1/2):115–136, 1997.
- [12] I. G. Kevrekidis, C. W. Gear, J. M. Hyman, P. G. Kevrekidis, O. Runborg, and C. Theodoropoulos. Equation-free, coarse-grained multiscale computation: Enabling microscopic simulators to perform system-level analysis. *Communications in Mathematical Sciences*, 1(4):715–762, 2003.
- [13] P. Lallemand and L.-S. Luo. Theory of the lattice Boltzmann method: Dispersion, dissipation, isotropy, Galilean invariance and stability. *Physical Review E*, 61(6):6546–6562, 2000.
- [14] K. Lust, D. Roose, A. Spence, and A. Champneys. An adaptive Newton-Picard algorithm with subspace iteration for computing periodic solutions. *SIAM Journal on Scientific Computing*, 19(4):1188–1209, 1998.
- [15] A. G. Makeev, D. Maroudas, and I. G. Kevrekidis. “Coarse” stability and bifurcation analysis using stochastic simulators: Kinetic Monte Carlo examples. *Journal of Chemical Physics*, 116(23):10083–10091, 2002.
- [16] A. G. Makeev, D. Maroudas, A. Z. Panagiotopoulos, and I. G. Kevrekidis. Coarse bifurcation analysis of kinetic Monte Carlo simulations: A lattice-gas model with lateral interactions. *Journal of Chemical Physics*, 117(18):8229–8240, 2002.
- [17] R. Mei, L.-S. Luo, P. Lallemand, and D. d’Humières. Consistent initial conditions for lattice Boltzmann simulations. to appear in *Computers & Fluids*, 2006.
- [18] Y. H. Qian, D. d’Humières, and P. Lallemand. Lattice BGK models for Navier-Stokes equation. *Europhysics Letters*, 17(6):479–484, 1992.
- [19] Y. H. Qian and S. A. Orszag. Scalings in diffusion-driven reaction  $A + B \rightarrow C$ : Numerical simulations by lattice BGK models. *Journal of Statistical Physics*, 81(1/2):237–253, 1995.
- [20] G. Samaey, D. Roose, and I. G. Kevrekidis. The gap-tooth scheme for homogenization problems. *Multiscale Modeling and Simulation*, 4(1):278–306, 2005.
- [21] G. J. Tee. Eigenvectors of compound-circulant and alternating circulant matrices. Technical Report 479, University of Auckland, Department of Mathematics, 2002.

- [22] C. Theodoropoulos, Y. H. Qian, and I. G. Kevrekidis. “Coarse” stability and bifurcation analysis using time-steppers: a reaction-diffusion example. *Proceedings of the National Academy of Sciences*, 97(18):9840–9843, 2000.
- [23] P. Van Leemput and K. Lust. Numerical bifurcation analysis of lattice Boltzmann models: a reaction-diffusion example. In M. Bubak, G. D. van Albada, P. M. Slood, and J. Dongarra, editors, *Computational Science – ICCS 2004*, volume 3039 of *Lecture Notes in Computer Science*, pages 572–579. Springer-Verlag, 2004.
- [24] P. Van Leemput, K. Lust, and I. G. Kevrekidis. Coarse-grained numerical bifurcation analysis of lattice Boltzmann models. *Physica D: Nonlinear Phenomena*, 210(1–2):58–76, 2005.
- [25] P. Van Leemput, W. Vanroose, and D. Roose. Numerical and analytical spatial coupling of a lattice Boltzmann model and a partial differential equation. Technical Report TW 445, Katholieke Universiteit Leuven, Department of Computer Science, 2005. accepted in *Model Reduction and Coarse-Graining Approaches for Multiscale Phenomena*, Springer-Verlag Lecture Notes.
- [26] C. Vandekerckhove, D. Roose, and K. Lust. Numerical stability analysis of an acceleration scheme for step size constrained time integrators. Technical Report TW 426, Katholieke Universiteit Leuven, Department of Computer Science, 2005. accepted in *Journal of Computational and Applied Mathematics*.
- [27] A. Zagaris, H. G. Kaper, and T. J. Kaper. Two perspectives on reduction of ordinary differential equations. *Mathematische Nachrichten*, 278(12-13):1629–1642, 2005.